Genomics

Molecular Cancer Research

Digital PCR-Based T-cell Quantification–Assisted Deconvolution of the Microenvironment Reveals that Activated Macrophages Drive Tumor Inflammation in Uveal Melanoma

Mark J. de Lange[1], Rogier J. Nell[1], Rajshri N. Lalai[1], Mieke Versluis[1], Ekaterina S. Jordanova[2,3], Gre P.M. Luyten[1], Martine J. Jager[1], Sjoerd H. van der Burg[4], Willem H. Zoutman[5], Thorbald van Hall[4], and Pieter A. van der Velden[1]

Abstract

Uveal melanoma progression can be predicted by gene expression profiles enabling a clear subdivision between tumors with a good (class I) and a poor (class II) prognosis. Poor prognosis uveal melanoma can be subdivided by expression of immune-related genes; however, it is unclear whether this subclassification is justified; therefore, T cells in uveal melanoma specimens were quantified using a digital PCR approach. Absolute T-cell quantification revealed that T-cell influx is present in all uveal melanomas associated with a poor prognosis. However, this infiltrate is only accompanied by differential immune-related gene expression profiles in uveal melanoma with the highest T-cell infiltrate. Molecular deconvolution of the immune profile revealed that a large proportion of the T-cell–related gene expression signature does not originate from lymphocytes but is derived from other immune cells, especially macrophages. Expression of the lymphocyte-homing chemokine CXCL10 by activated macrophages correlated with T-cell infiltration and thereby explains the correlation of T-cell numbers and macrophages. This was validated by *in situ* analysis of CXCL10 in uveal melanoma tissue with high T-cell counts. Surprisingly, CXCL10 or any of the other genes in the activated macrophage-cluster was correlated with reduced survival due to uveal melanoma metastasis. This effect was independent of the T-cell infiltrate, which reveals a role for activated macrophages in metastasis formation independent of their role in tumor inflammation.

Implications: The current report uses an innovative digital PCR method to study the immune environment and demonstrates that absolute T-cell quantification and expression profiles can dissect disparate immune components. *Mol Cancer Res; 16(12); 1902–11. ©2018 AACR.*

Introduction

Uveal melanoma is the most common intraocular neoplasm in adults with an incidence of 6 to 8 per million annually in Caucasians (1). Uveal melanoma presents as a genetically homogenous disease in the sense that the vast majority shares the same driver mutations (GNAQ/11; refs. 2, 3). Downstream oncogenic signaling pathways include the ERK pathway via PKC and the Hippo pathway via YAP activation (4, 5). For years, it has been known that uveal melanomas that metastasize significantly differ both in their genetic and their phenotypic make up, from the ones that do not metastasize. Early studies showed recurrent genomic abnormalities that allowed clustering of tumors into prognostic classes (6–8). Monosomy of chromosome 3 and gain of chromosome 8q discriminate between good and poor prognosis (9–11). More recently, an advanced approach of classifying uveal melanoma was revealed. On the basis of genome-wide gene expression analysis, tumors were assigned to prognostic classes (class I and class II) that overlap largely with the genomic classification (12). The former classification is based on hundreds of differentially expressed genes that may also provide insight into the biology of uveal melanoma. Recently, we and others demonstrated that a part of the uveal melanoma with a poor prognosis is characterized by an extensive immune infiltrate (6, 13). Besides T-cell markers, macrophage markers were recognized in the expression profiles of uveal melanoma with metastatic potential. Macrophage activation has been shown to precede T-cell infiltration in uveal melanoma progression (14). To further investigate the mechanisms of uveal melanoma inflammation, the expression profile was analyzed for the inflammatory compartment. For this purpose, absolute T-cell counts were integrated with uveal melanoma expression profiles. The resulting T-cell–related genes were compared with a range of immune cells to identify immune cells in the tumor microenvironment. By

[1]Department of Ophthalmology, LUMC, Leiden, the Netherlands. [2]Department of Pathology, LUMC, Leiden, the Netherlands. [3]Center for Gynecologic Oncology Amsterdam, VUmc, the Netherlands. [4]Department of Medical Oncology, LUMC, Leiden, the Netherlands. [5]Department of Dermatology, LUMC, Leiden, the Netherlands.

Note: Supplementary data for this article are available at Molecular Cancer Research Online (http://mcr.aacrjournals.org/).

M.J. de Lange and R.J. Nell contributed equally to this article.

Corresponding Author: Pieter A. van der Velden, Leiden University Medical Center, Albinusdreef 2, Leiden, Zuid-Holland 2333ZA, the Netherlands. Phone: 317-1526-6258; Fax: 317-1526-8286; E-mail: velden@lumc.nl

doi: 10.1158/1541-7786.MCR-18-0114

using profiles of both naïve and activated immune cells, we could infer that activated macrophages are pivotal in T-cell infiltration. Combined, we show that by using absolute T-cell counts, expression profiles of heterogeneous tissue can be effectively dissected into different immune components.

Materials and Methods

Tumor material was obtained from 64 enucleated eyes of uveal melanoma patients that had been enucleated at the Leiden University Medical Center, Leiden, the Netherlands, between 1999 and 2008. This study was approved by the Medical Ethics Committee of the Leiden University Medical Center. Tumor material was handled according to the Dutch National Ethical Guidelines (Code for Proper Secondary Use of Human Tissue) and the tenets of the Declaration of Helsinki (World Medical Association of Declaration 2013; ethical principles for medical research involving human subjects). None of the tumors had prior treatment, and only tumors with a follow-up time of at least 5 years were used. The maximum follow-up was 14 years. The average age at enucleation was 60.6 years (range, 13–88); 33 patients were male and 31 were female.

Tumor material was snap frozen using 2-methyl butane, and RNA and DNA were isolated using the RNeasy Mini Kit and QIAamp DNA Mini Kit, respectively (both Qiagen), from 20 sections of 20 μm according to the manufacturer's guidelines.

Gene expression

Gene expression analysis was performed as published before (6). In short, the Illumina HumanHT-12 v4 chip containing 47,000 probes across the whole genome was used. Supervised cluster analysis was used to identify which genes were responsible for the subdivision of the tumors in classes. For differences between subgroups, that is, I versus II, a correction was made for differences between IIa and IIb classified as a log fold change smaller than −0.5 or greater than 0.5 and a *P*-value smaller than 0.05. Because gene expression data have been obtained in two batches, a batch effect correction was applied. The R packages used were: "ber" for batch correction and "lumi" for unsupervised clustering.

Genetic T-cell quantification

To quantify T cells in tumor samples, a dPCR assay was developed directed at a specific locus of the TCR-β gene; located between gene segments Dβ1 and Jβ1.1, and from now on called Δ*B*. This particular part of the gene is biallelically deleted by T-cell receptor rearrangements during T-cell maturation. Consequently, peripheral T cells are lacking Δ*B* compared with other cell types (somatic loss of germline DNA). This genetic dissimilarity can be utilized in a basic copy number variation (CNV) dPCR assay in order to quantify T cells in the presence of other cell types, like uveal melanoma (tumor) cells. Because a stable genomic reference is essential in this determination, $\frac{[\Delta B]}{[\text{REFERENCE}]}$ was calculated for three different reference genes: TTC5 (chr. 14), TERT (chr. 5), and VOPP1 (chr. 7). The average of the two closest ratios was used in the following formula:

$$\text{T-cell fraction} = 1 - \text{average}\frac{[\Delta B]}{[\text{REFERENCE}]}$$

Although the target gene segment Δ*B* is located at a locus not frequently mutated in uveal melanoma cells, copy number alterations in tumor cells may give rise to a distortion of our calculations. It is possible to correct for this by using the following formula:

$$\text{Adjusted T-cell fraction} = \text{average}\frac{[\text{VOPP1}]}{[\text{REFERENCE}]} - \text{average}\frac{[\Delta B]}{[\text{REFERENCE}]}$$

In those cases where chromosome 7 shows an obvious loss or gain (defined by a concordant copy number alteration > 0.075 seen in $\frac{[\text{VOPP1}]}{[\text{TTC5}]}$ and $\frac{[\text{VOPP1}]}{[\text{TERT}]}$), we chose to determine T-cell fractions according to this formula. In those calculations, VOPP1 was not used as reference gene. Calculations per tumor are outlined in Supplementary Table S2.

The ddPCR was performed using ddPCR Supermix for probes (Bio-Rad) in 20 μL with 50 ng of DNA resulting in 0.75 copies per droplet (CPD) of haploid genomes after partitioning into 20,000 droplets.

DNA restriction digestion was performed using HaeIII directly in the ddPCR reaction solution according to the protocol supplied by Bio-Rad. Droplets were generated using an AutoDG System (Bio-Rad) and droplet emulsion was transferred to a 96-well PCR plate for amplification in a T100 Thermal Cycler (Bio-Rad). Cycle parameters were as follows: Enzyme activation for 10 minutes at 95°C; denaturation for 30 seconds at 94°C, annealing and extension for 1 minute at 60°C for 40 cycles; enzyme deactivation for 10 minutes at 98°C; infinite cooling at 12°C. Ramp rate for all cycles was 2°C/sec. Cycled droplets were stored at 4°C to 12°C until reading. Positive and negative droplets were measured as a CNV1 experiment using a QX200 Droplet Reader (Bio-Rad). Primers and probes are proprietary of Bio-Rad except for the primers and probes for TRB, which have been published before (15). In Supplementary Table S3, the amplicon sequences are provided.

BIOGPS method

Obtained gene expression profiles from uveal melanoma samples represent a mixture of cell types, that is, melanoma cells and stromal cells. We developed a computational approach to dissect which cell types contribute to the expression signatures.

At the basis of our *in silico* analysis lies the selection of genes of interest for which the expression level is positively correlated with increased T-cell fraction in the class II uveal melanoma samples ($n = 38$). Pearson correlation test was used and $r > 0.5$ and $P < 0.001$ were considered to be significant.

The publicly available datasets GeneAtlas U133A, gcrma (16), and Primary Cell Atlas (17) on the BioGPS-site were used to obtain cell-type–specific gene expression patterns for our selected genes (18–20). Hierarchical cluster analysis and principal component analysis (PCA) revealed cell-specific expression patterns in our gene selection. The following R packages were used: "mygene" for obtaining gene information and "pheatmap," "dendsort," and "ggplot2" for visualizing data.

Immunofluorescent staining

Phenotypic characterization of lymphocytes was performed using triple fluorescent immunostaining. A previously developed technique for simultaneous immunofluorescence (IF) staining of different epitopes was applied to 4-μm formalin-fixed, paraffin-embedded tissue sections. In brief, deparaffinized and EDTA

antigen retrieval-treated sections were stained by a mixture of the following primary antibodies: anti-CD8 (mouse monoclonal IgG1; Dako-Agilent), melan A (mouse monoclonal; Novus Biologicals, LLC), CXCL10 (rabbit polyclonal; Antibodies-online), CD14 (mouse monoclonal IgG2a; Abcam), CD163 (mouse monoclonal IgG1; Novocatra). As secondary antibodies to visualize the lymphocytes, a combination of fluorescent antibody conjugates goat anti-rabbit IgG-Alexa Fluor 546, goat anti-mouse IgG2b-Alexa Fluor 647, goat anti-mouse IgG1-Alexa Fluor 488 (all three from Molecular Probes; Invitrogen), and goat anti-rabbit-Alexa Fluor 647, goat anti-mouse IgG2a-Alexa Fluor 546, and goat anti-mouse IgG1-Alexa Fluor 488 (all three from Life Technologies) was used. Antibodies were used as described previously (21). Images were captured with a confocal laser scanning microscope (LSM510; Carl Zeiss Meditec) in a multitrack setting. A microscope objective (PH2 Plan-NEOFluar 25×/0.80 Imm Korr; Zeiss) was used. T cells were manually counted using the LSM 5 Image Examiner software and represented as the number of cells per mm^2 for each slide (average of five 250× images).

Statistical analysis

For gene expression, deconvolution, and statistical analyses, the programming language R was used [R Core Team (2016), R: A language and environment for statistical computing, R Foundation for Statistical Computing, Vienna, Austria]. Detailed methods for analysis are provided in Supplementary Methods.

Results

Uveal melanoma subclassification reveals an immune phenotype

With gene expression profiles, uveal melanoma can be easily subdivided into different prognostic classes (12, 22). Class I mainly consists of tumors with a good prognosis, whereas class II represents tumors with a poor prognosis (Fig. 1A). On the basis of the most differentially expressed genes, we recognized two subclasses (IIa/IIb) in class II uveal melanoma (6). These subclasses however do not present with a survival difference (Fig. 1A). High expression of immune-related genes in class IIb uveal melanoma suggests that these tumors are inflamed, whereas class IIa uveal melanoma tumors do not include this phenotype (Fig. 1B).

Although gene expression profiles are helpful in exploring the immune infiltrate, they do not provide an immune cell count. The underlying reason may be that cell-specific markers such as CD4 and CD8 are regulated during immune reactions. This makes CD4 and CD8 expression useful to describe the T-cell populations, rather than for T-cell quantification. CD3 expression is marginally regulated during immune responses compared to CD4 and CD8

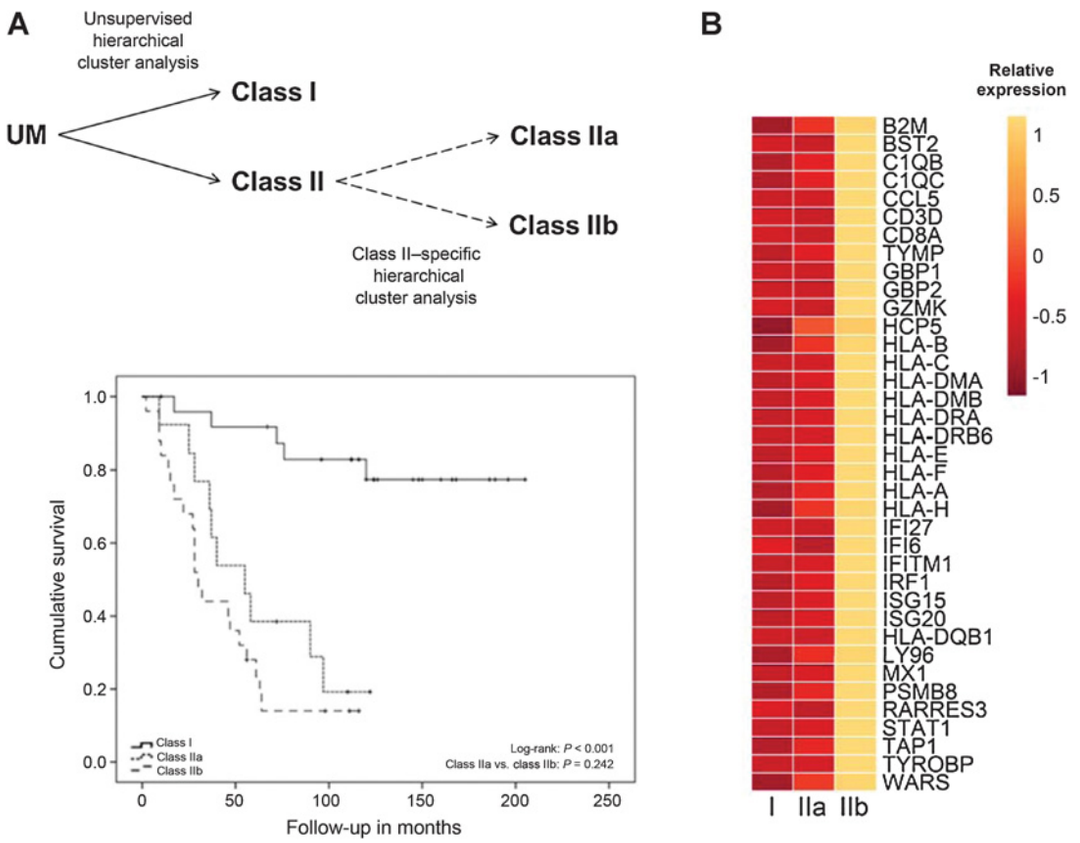

Figure 1.

Classification of uveal melanoma using gene expression analysis. **A,** Unsupervised hierarchical clustering of genome-wide expression levels divides uveal melanoma into two prognostic classes (class I and class II). By supervised clustering of the classifier genes, class II is even further subdivided into class IIa and class IIb. Subdivision in class IIa and class IIb does not result in a survival difference (6). **B,** The genes that define class IIb reveal an immunologic signature.

and therefore more appropriate to enumerate the T-cell infiltrate. To define the extent of the immune cell infiltration in uveal melanoma more accurately, we quantified T cells in uveal melanoma DNA specimens from which the gene expression profiles were also obtained.

Digital PCR reveals T-cell infiltration in the whole of class II uveal melanoma

On the basis of somatic rearrangements of the T-cell receptor genes, T cells can be distinguished from other cells at the genomic and RNA level. The number of possible rearrangements is however innumerable, and amplification of every possible T-cell receptor requires many assays (23). The complexity of the TCR genes therefore hampers accurate measurement and analysis at genomic level and the gene expression level. Instead of counting each individual rearrangement, we used an alternative amplification method for quantification that depends on a DNA sequence (ΔB). This sequence is deleted in both alleles of lymphocytes during early T-cell maturation and therefore the marker of choice for counting T cells (15, 24).

With dPCR, T-cell numbers were quantified in the tumor mass of 64 uveal melanomas that were previously analyzed with gene expression arrays. Significantly higher T-cell fractions were observed in class IIb tumors compared with class IIa and class I tumors (Fig. 2A). However, elevated T-cell counts can also be found in class IIa, compared with class I uveal melanoma. This is in contrast to gene expression analysis of CD3, which did not reveal significant differences between class I and class IIa (Fig. 2B). The lack of differential expression of CD3 between class I and class IIa likely marks the reduced sensitivity and specificity of gene expression arrays compared with the DNA-based T-cell count. Significant correlations between genomic T-cell counts and gene expression of CD3 were nevertheless observed (Fig. 2C). To assess the degree to which T cells contribute to the gene expression profile, we systematically correlated T-cell number and gene expression profiles of classifier genes.

Integration of T-cell count with the expression profile of uveal melanoma reveals structure of the immune environment

Instead of investigating the expression profile for immune cell markers, we investigated the degree to which T cells contribute directly or indirectly to the expression profile of class II uveal melanoma. Therefore, we reversed the analysis and performed supervised cluster analysis on the basis of the T-cell count. The correlation with T-cell count was determined for 1,538 (log-fold change >0.5) probe sets, which are differentially expressed between class I and class II. This revealed that 60 genes of the class II classifier are positively correlated with T-cell count ($R > 0.5$, $P < 0.05$; Fig. 3A; Supplementary Table S1). Among these T-cell classifier genes are obligate T-cell markers such as CD3 and CD8. Also lymphocyte-attracting chemokines like CCL5 are expressed by T cells and found to be present in the T-cell classifier (25). Comparison of the expression profiles with 35 expression profiles of naïve and activated immune cells indicated that the majority of

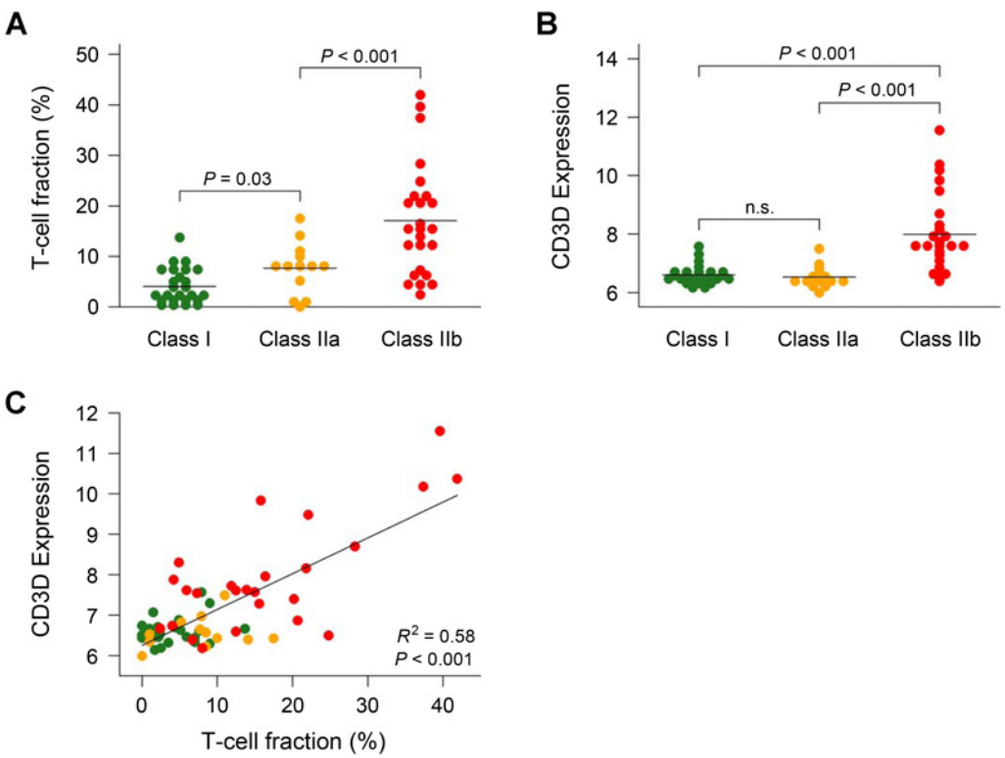

Figure 2.

Quantification of T cells in 64 uveal melanomas divided over the three gene expression classes. **A,** Significantly higher T-cell fractions are found in class IIa and class IIb compared with class I and class IIa, respectively. **B,** CD3D expression (*y*-axis) in the classes, with a significant expression difference between class IIa and class IIb but no significant expression difference between class I and class IIa. **C,** Correlation of CD3D expression (*y*-axis) with T-cell count in the three expression classes.

T-cell–correlated genes is actually not expressed by T cells (Fig. 3B). The myeloid lineage of immune cells was found to contribute considerably to the T-cell classifier. This is illustrated by the correlation between T-cell count and macrophage markers such as CD14 ($R = 0.484$, $P = 0.002$), CD86 ($R = 0.70$, $P < 0.05$), and CSF1R ($R = 0.606$, $P < 0.001$). However, the variability of the correlation between macrophage markers and T-cell count, or even absence of a correlation (CD68, $R = 0.196$, $P = 0.239$), indicates that macrophage polarization is highly dynamic. Moreover, the variable correlation of macrophage marker expression with T-cell count indicates that specific subtypes of macrophages are present in inflamed uveal melanoma. With PCA, the T-cell classifier converged into 4 clusters that represent different cell populations (Fig. 3C). The most distinct gene cluster contained

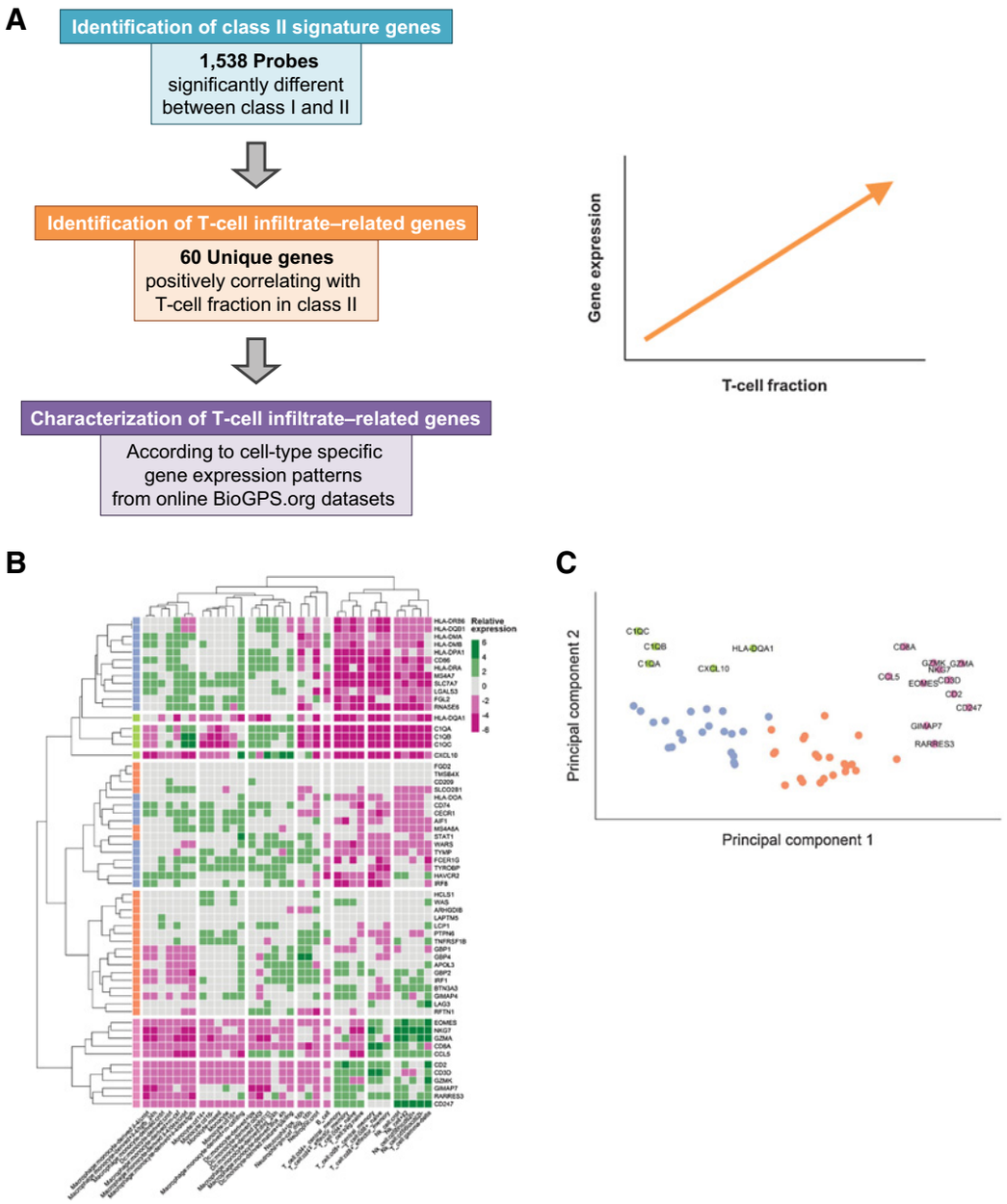

Figure 3.

Deconvolution of the immune phenotype of uveal melanoma with T-cell count. **A,** Analysis of the uveal melanoma classifier genes for T-cell–related genes consisted of two additional steps; a correlation between T-cell count and gene expression level and analysis of cell-type distribution of differentially expressed genes. **B,** Relative expression levels of the 60 T-cell–correlated genes in a range of immune cells. **C,** T-cell–related genes dispersed in four cell types after clustering for cell-type distribution. In blue the monocyte/macrophage cluster, in green the activated macrophages, in pink the activated cytotoxic T cells, and in orange an undefined population of immune cells.

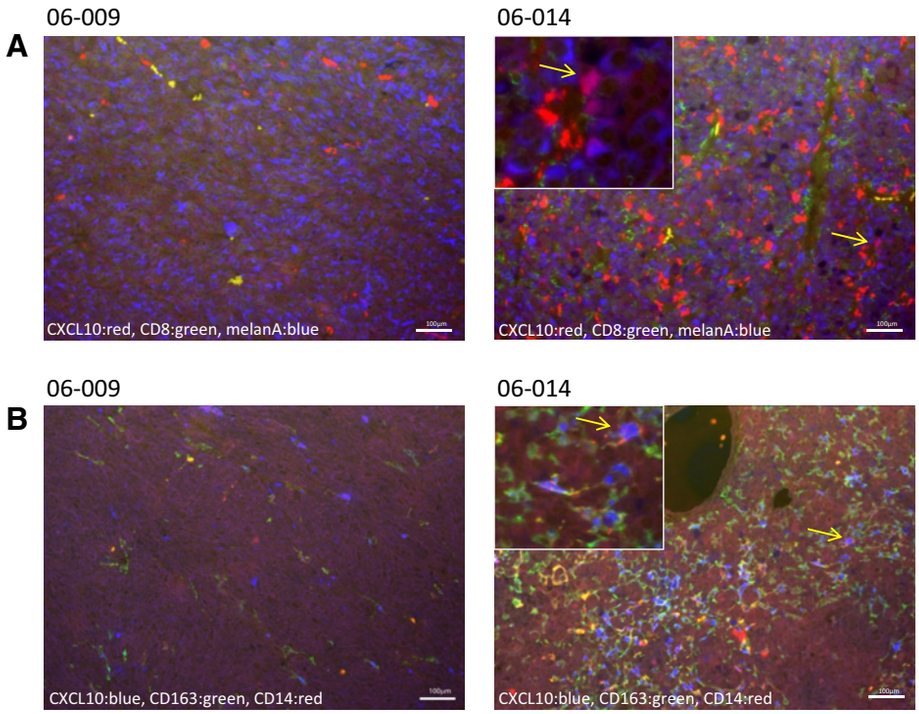

Figure 4.
Multiplex immunofluorescent staining of uveal melanoma samples with a high (06-014: 42%) and low (06-009: 0%) calculated T-cell fraction. CXCL10 colocalization with T cells and macrophages in uveal melanoma. **A,** CXCL10 (red) does not colocalize with T cells (CD8: green) and hardly ever with melanoma cells (melanA: blue). Zoomed in picture insert indicates melanoma cells that express CXCL10. **B,** CXCL10 (blue) colocalizes with macrophages (CD163: green, CD14: red) of varying polarization.

expression profiles of macrophages that had been activated with classic immune activators like LPS and IFNγ. Another prominent cluster corresponded to the profile of activated CD8-positive T cells, as can be witnessed by high granzyme expression. The lymphocyte-attracting chemokine CXCL10 was highly expressed in the activated macrophage gene cluster, and may be functionally related to T-cell infiltration in uveal melanoma (Fig. 3B and C). Expression of CXCL10 by macrophages was investigated in uveal melanoma tissue with two triple staining procedures. Either T-cell or macrophage markers were analyzed alongside a melanocyte marker and CXCL10 expression. This confirmed high CXCL10 expression by macrophages in uveal melanoma with high T-cell counts. Although staining with macrophage markers (CD14, CD163) revealed that macrophages are the origin of CXCL10 expression. Although uveal melanoma cells also occasionally displayed CXCL10 expression, strong staining was uniquely observed in macrophages that express CD163 (Fig. 4A and B; Table 1). Combined, this displays an active immune response in part of the uveal melanoma, and the question emerges whether this results in a clinical response.

Clinical consequence of the immunologic phenotype

Previously, we reported that the class IIa and class IIb uveal melanomas presented with similar prognosis (Fig. 1A). On the basis of that, we claimed that presence or absence of an immune infiltrate did not influence disease outcome in uveal melanoma (6). With two immune cell populations in uveal melanoma defined, we evaluated the role of T-cell count and activated macrophages in the development of uveal melanoma metastasis separately. We analyzed this in a molecular uveal melanoma risk model, to which we added T-cell count as well as expression markers for T-cell phenotype (CD4, CD8) and CXCL10 expression as marker for activated macrophages. In this model, monosomy 3 and chromosome 8q gain were significantly correlated with survival (Table 2). T-cell count did not contribute to survival (Fig. 5), and neither did the expression of the T-cell markers (CD4, CD8). CXCL10 as a marker for activated macrophages did surprisingly contribute to the survival risk of uveal melanoma in this complex model. Thereby, it was shown to represent an independent risk factor that is not confounded by monosomy 3, gain of 8q or T-cell count.

Discussion

Molecularly, uveal melanomas can be easily divided into different prognostic classes (class I and class II) based on their genome-wide gene expression (12, 22). Recently, our gene expression analysis of 64 uveal melanomas revealed an additional subdivision. With supervised cluster analysis of the classifier genes, class II uveal melanoma was subdivided into class IIa and class IIb. Genes that were differentially expressed between these classes, and thus responsible for this subdivision, were functionally annotated to be related to the immune system. Expression of IFN signature genes like CD2, CD3D, CCL5, and CXCL10 reflect an ongoing tumor inflammation (26). Moreover, expression of cytolytic genes (GZMA, GZMK, and NGK7) in the same cluster supported that the T cells are cytotoxic effector cells. Class IIa uveal melanoma contained little involvement of the immune system as opposed to class IIb uveal melanoma, in which an inflammatory phenotype was observed (6). This subdivision is reminiscent of the class 3 and class 4 classification that the TCGA consortium recently described (13). It is, however, the question whether class II subclassification is warranted on molecular merits or that it is solely based on the degree of immune infiltration. The TCGA consortium estimated the leukocyte fraction with methylation profiles that were correlated to histopathologically determined leukocyte fractions (27). With this approach, leukocytes were

Table 1. Histologic T-cell and CXCL10 counts

UM	Class	T-cell counts (mm^2)	CXCL10 Macrophages	CXCL10 Tumor cells
05–005	IIb	5.61	Low	Low
05–020	I	18.00	Intermediate	Intermediate
05–046	IIa	5.55	Intermediate	High
05–061	IIa	8.31	Low	Intermediate
06–008	IIb	75.07	High	Low
06–009	IIa	2.77	Low	High
06–014	IIb	456.71	High	High
06–041	IIb	0.46	Low	Low
07–007	I	217.13	High	High
08–029	IIb	34.77	High	Low

Abbreviation: UM, uveal melanoma.

found to be elevated in class 4, similar to what we observed with expression markers for T cells in class IIb uveal melanoma (6). Although expression profiles and methylation profiles may be related to cell fractions, they do not represent absolute cell numbers. Expression and methylation profiles rather identify cell fractions that are present in the tumor tissue. Alternatively, absolute quantification of immune cells can be achieved by flow sort analysis of tumor material, but this is difficult and has not been applied to uveal melanoma. T-cell and macrophage counting in tissue with IHC has been used as an accessible alternative and this confirmed wide ranging T-cell and macrophage infiltration in uveal melanoma (28, 29). In the inflamed tumors the T cells and macrophages are spread throughout the tumor and thereby show that immune cell invasion is not limited to a specific histologic structure or tissue (Fig. 4). Moreover, integration of T cell and macrophage staining with the molecular progression model of uveal melanoma revealed that macrophage infiltration precedes T-cell infiltration in tumor inflammation (6, 14). We integrated absolute T-cell counts with expression profiles of uveal melanoma, to investigate the biologic mechanisms. We quantified T cells with a DNA-based quantitative method that would otherwise require fresh cell homogenates and flow cytometry (15). Integration of RNA expression profiles and DNA-based T-cell counts in the same tissue revealed that T-cell fractions can exceed way over one tenth of the tumor mass. The highest T-cell fractions were observed in class IIb uveal melanoma, and the median T-cell fraction was almost twice as high as in class IIa (15.6% and 8.0%, respectively). Class I uveal melanoma, on the other hand, presents the lowest T-cell fraction (5.1%), and combined this suggests an accumulation of T cells during uveal melanoma progression (Fig. 2A). Remarkably, the elevated T-cell numbers in class IIa were not reflected by an increase in T-cell marker gene expression (Fig. 2B). We suppose that dilution of the gene expression profiles of reduced T-cell fractions (<10%) in class IIa obscured the contribution of T cells to the complete profile. Alternative explanation could be that CD3 is regulated during immune activation, although this is not evident from the reference database that we use (17). In class IIa, 8% T cells were found compared with 5% in class I and it is questionable whether expression array analysis can distinguish this difference. Because of the absolute quantification with digital PCR approach, a gradual increase of T-cell infiltrate could now be recognized. Although the gene expression analysis initially suggested immune infiltration in specifically class IIb uveal melanoma, absolute T-cell quantification now showed that T-cell influx occurs in the whole of class II uveal melanoma but is highest in class IIb. Therefore, subclassification of class II uveal melanoma with expression profiles appears to be based on a quantitative difference in T-cell infiltration.

Earlier reports from our research group indicated that the immune system is involved in uveal melanoma with poor prognosis (28, 29). Our analyses revealed an extensive CD8-positive T-cell infiltrate in uveal melanoma and validated immune involvement in class II uveal melanoma with a poor prognosis. However, both the gene expression based inflammatory phenotype of class IIb uveal melanoma (Fig. 1B), and T-cell count in the whole of our uveal melanoma panel (Table 2), did not correlate with survival. Indeed, class II uveal melanoma contains more T-cell infiltrate than class I uveal melanoma, but when analyzed in a multivariate statistical model, including the known genetic risk factors, no added risk was revealed for T-cell numbers. This also did not depend on T-cell differentiation, as both CD4 expression as well as CD8 expression behaved neutrally in our risk model (Table 2).

The question remains how the immune infiltrate in uveal melanoma should be further interpreted. To investigate this, we combined T-cell quantifications with the gene expression profile of each corresponding tumor. The result of this analysis, a list of correlated genes (directly or indirectly related to the T-cell immune infiltration), was integrated with publicly available cell-type–specific gene expression profiles. This led to the remarkable conclusion that most of these T-cell count-related genes are

Table 2. Survival analysis of uveal melanoma

Variables in the equation	*B*	*P*-value	Exp(*B*)
T cell fraction	0.008	0.726	1.008
Chromosome 6p copy number	0.239	0.529	1.269
Chromosome 3 copy number	−1.929	0.001	0.145
Chromosome 8q copy number	0.321	0.018	1.379
CD8 expression	−0.282	0.209	0.754
CD4 expression	−0.032	0.969	0.968
CXCL10 expression	0.578	0.017	1.782

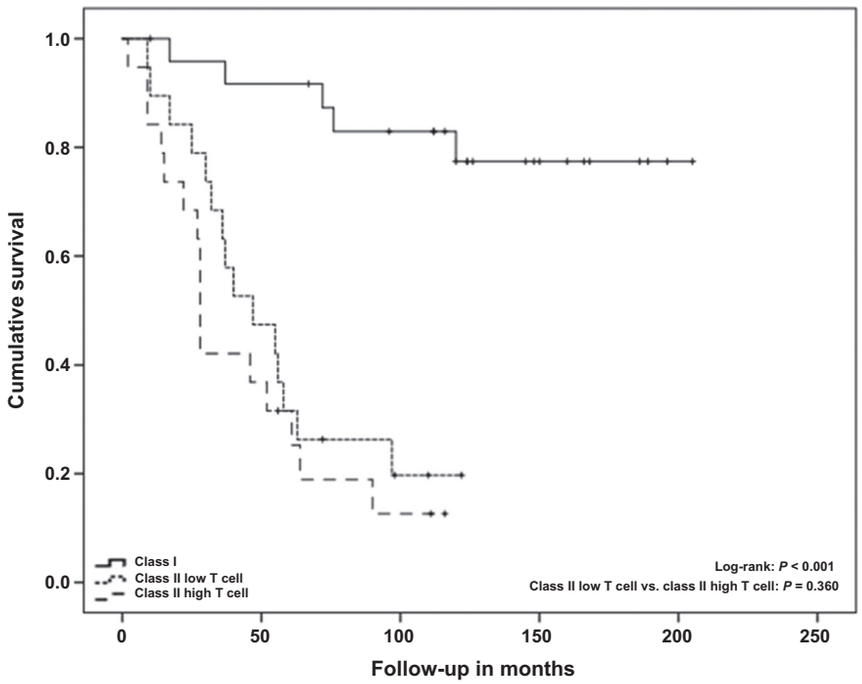

Figure 5.
Survival analysis of uveal melanoma containing high numbers of T cells did not show a benefit for T-cell infiltrate. Class I presents with a good prognosis, whereas class II uveal melanomas are correlated with a poor prognosis. Subdivision of class II in low and high T-cell–infiltrated uveal melanoma does not make a difference in survival.

actually expressed by other cells in the immune compartment, mostly monocyte derived.

Deconvolution of the genes that are correlated with T-cell count indicated that activated macrophages contribute considerably to the overall uveal melanoma immune infiltrate as well as activated cytotoxic T cells. The fact that this activated immune infiltrate does not result in an overt immune response, and consequently an improved prognosis, suggests that immunosuppression is involved. Therefore, the eye is an immune privileged organ, making it a unique organ and a favorable location for allograft residence (30). Moreover, the blood–retina barrier, which is characterized by tight junctions in the retinal pigmented epithelial layer, actively blocks the influx of immune cells from the surrounding tissue (31). Combined, this possibly reflects a negative selection pressure, as immune reactions in the eye could have detrimental effects on delicate structures, leading to impaired vision (32, 33). The presence of activated immune cells in uveal melanoma is therefore remarkable and may be a consequence of uveal melanoma development. There is, however, no correlation to the development of metastases, and this may suggest that immune infiltration can be regarded an epiphenomenon of progression that has no effect on survival of patients However, preliminary analysis indicates that activated macrophages, as marked by CXCL10 expression, may be involved in metastasis (Fig. 5, Table 2).

Interestingly, the role of CXCL10 in uveal melanoma has been described before, and this chemokine showed to be present in uveal melanoma cells and upregulated in a T-cell–rich environment (25, 34, 35). CXCL10 staining of uveal melanoma sections in our cohort indicated that CXCL10 is present in some tumor cells but is predominantly found in macrophages (Fig. 4B). Although the intensity levels of CXCL10 and macrophage marker gene expression varied in uveal melanoma with high T-cell counts, high levels of CXCL10 expression were restricted to the macrophages. Remarkably, although T-cell count and CXCL10 are highly correlated, in survival analysis, CXCL10 expression was correlated with a considerably increased risk while T-cell count was not correlated to an increased risk. This suggests that besides attracting T cells by expressing CXCL10, macrophages also contribute to uveal melanoma progression in another way. Possibly by stimulating uveal melanoma cell proliferation and extravasation in the same way that skin melanoma cells with ectopic expression of the CXCL10 receptor CXCR3 are stimulated (36, 37). It is, however, unlikely that the same mechanism applies to uveal melanoma, because CXCR3 was not differentially expressed between the uveal melanoma classes (Supplementary Table S1). Possibly other chemokine and chemokine receptor combinations drive tumor growth and progression in uveal melanoma (38).

With absolute T-cell quantification, we managed to take the first step in deconvolution of the immune compartment in uveal melanoma. Thereby, we revealed increasing numbers of activated T cells and activated macrophages in uveal melanoma with poor prognosis. With CXCL10 expression by macrophages in uveal melanoma, we revealed a possible underlying mechanism of T-cell infiltration. On the basis of survival analysis, we hypothesize that T-cell infiltration is an epiphenomenon of a macrophage-driven metastatic process. A further deconvolution of the macrophage-related expression profile will be the approach to reveal the cells and the involved mechanisms.

Disclosure of Potential Conflicts of Interest

No potential conflicts of interest were disclosed.

Authors' Contributions

Conception and design: M.J. de Lange, R.J. Nell, W.H. Zoutman, P.A. van der Velden

Development of methodology: M.J. de Lange, R.J. Nell, E.S. Jordanova, W.H. Zoutman
Acquisition of data (provided animals, acquired and managed patients, provided facilities, etc.): M.J. de Lange, R.J. Nell, M. Versluis, E.S. Jordanova, M.J. Jager
Analysis and interpretation of data (e.g., statistical analysis, biostatistics, computational analysis): M.J. de Lange, R.J. Nell, M. Versluis, E.S. Jordanova, S.H. van der Burg, T. van Hall
Writing, review, and/or revision of the manuscript: M.J. de Lange, R.J. Nell, R.N. Lalai, E.S. Jordanova, M.J. Jager, S.H. van der Burg, W.H. Zoutman, T. van Hall, P.A. van der Velden
Administrative, technical, or material support (i.e., reporting or organizing data, constructing databases): M.J. de Lange, R.J. Nell, R.N. Lalai, M. Versluis, M.J. Jager
Study supervision: G.P.M. Luyten, P.A. van der Velden

Acknowledgments

The authors would like to thank A.W. Langerak for helpful discussion on T-cell genetics and D. van Steenderen for counting T cells. N.A. Gruis and T. Larsen are acknowledged for proofreading of this manuscript. R.J. Nell is supported by the European Union's Horizon 2020 research and innovation program under grant agreement no. 667787 (UM Cure 2020 project).

The costs of publication of this article were defrayed in part by the payment of page charges. This article must therefore be hereby marked *advertisement* in accordance with 18 U.S.C. Section 1734 solely to indicate this fact.

Received February 2, 2018; revised April 19, 2018; accepted July 20, 2018; published first August 9, 2018.

References

1. Singh AD, Turell ME, Topham AK. Uveal melanoma: trends in incidence, treatment, and survival. Ophthalmology 2011;118:1881–5.
2. Van Raamsdonk CD, Bezrookove V, Green G, Bauer J, Gaugler L, O'Brien JM, et al. Frequent somatic mutations of GNAQ in uveal melanoma and blue naevi. Nature 2009;457:599–602.
3. Van Raamsdonk CD, Griewank KG, Crosby MB, Garrido MC, Vemula S, Wiesner T, et al. Mutations in GNA11 in uveal melanoma. N Engl J Med 2010;363:2191–9.
4. Feng X, Degese MS, Iglesias-Bartolome R, Vaque JP, Molinolo AA, Rodrigues M, et al. Hippo-independent activation of YAP by the GNAQ uveal melanoma oncogene through a trio-regulated rho GTPase signaling circuitry. Cancer Cell 2014;25:831–45.
5. Sagoo MS, Harbour JW, Stebbing J, Bowcock AM. Combined PKC and MEK inhibition for treating metastatic uveal melanoma. Oncogene 2014;33:4722–3.
6. de Lange MJ, van Pelt SI, Versluis M, Jordanova ES, Kroes WG, Ruivenkamp C, et al. Heterogeneity revealed by integrated genomic analysis uncovers a molecular switch in malignant uveal melanoma. Oncotarget 2015;6:37824–35.
7. McNamara M, Felix C, Davison EV, Fenton M, Kennedy SM. Assessment of chromosome 3 copy number in ocular melanoma using fluorescence *in situ* hybridization. Cancer Genet Cytogenet 1997;98:4–8.
8. Speicher MR, Prescher G, du Manoir S, Jauch A, Horsthemke B, Bornfeld N, et al. Chromosomal gains and losses in uveal melanomas detected by comparative genomic hybridization. Cancer Res 1994;54:3817–23.
9. Prescher G, Bornfeld N, Hirche H, Horsthemke B, Jockel KH, Becher R. Prognostic implications of monosomy 3 in uveal melanoma. Lancet 1996;347:1222–5.
10. Patel KA, Edmondson ND, Talbot F, Parsons MA, Rennie IG, Sisley K. Prediction of prognosis in patients with uveal melanoma using fluorescence in situ hybridisation. Br J Ophthalmol 2001;85:1440–4.
11. Scholes AG, Damato BE, Nunn J, Hiscott P, Grierson I, Field JK. Monosomy 3 in uveal melanoma: correlation with clinical and histologic predictors of survival. Invest Ophthalmol Vis Sci 2003;44:1008–11.
12. Onken MD, Worley LA, Ehlers JP, Harbour JW. Gene expression profiling in uveal melanoma reveals two molecular classes and predicts metastatic death. Cancer Res 2004;64:7205–9.
13. Robertson AG, Shih J, Yau C, Gibb EA, Oba J, Mungall KL, et al. Integrative analysis identifies four molecular and clinical subsets in uveal melanoma. Cancer Cell 2017;32:204–20.
14. Gezgin G, Dogrusoz M, van Essen TH, Kroes WG, Luyten GP, van der Velden PA, et al. Genetic evolution of uveal melanoma guides the development of an inflammatory microenvironment. Cancer Immunol Immunother 2017;66:903–12.
15. Zoutman WH, Nell RJ, Versluis M, van Steenderen D, Lalai RN, Out-Luiting JJ, et al. Accurate quantification of T cells by measuring loss of germline T-cell receptor loci with generic single duplex droplet digital PCR assays. J Mol Diagn 2017;19:236–43.
16. Su AI, Wiltshire T, Batalov S, Lapp H, Ching KA, Block D, et al. A gene atlas of the mouse and human protein-encoding transcriptomes. Proc Natl Acad Sci U S A 2004;101:6062–7.
17. Mabbott NA, Baillie JK, Brown H, Freeman TC, Hume DA. An expression atlas of human primary cells: inference of gene function from coexpression networks. BMC Genomics 2013;14:632.
18. Wu C, Jin X, Tsueng G, Afrasiabi C, Su AI. BioGPS: building your own mash-up of gene annotations and expression profiles. Nucleic Acids Res 2016;44:D313–6.
19. Wu C, Macleod I, Su AI. BioGPS and MyGene.info: organizing online, gene-centric information. Nucleic Acids Res 2013;41:D561–5.
20. Wu C, Orozco C, Boyer J, Leglise M, Goodale J, Batalov S, et al. BioGPS: an extensible and customizable portal for querying and organizing gene annotation resources. Genome Biol 2009;10:R130.
21. Heeren AM, Punt S, Bleeker MC, Gaarenstroom KN, van der Velden J, Kenter GG, et al. Prognostic effect of different PD-L1 expression patterns in squamous cell carcinoma and adenocarcinoma of the cervix. Mod Pathol 2016;29:753–63.
22. Tschentscher F, Husing J, Holter T, Kruse E, Dresen IG, Jockel KH, et al. Tumor classification based on gene expression profiling shows that uveal melanomas with and without monosomy 3 represent two distinct entities. Cancer Res 2003;63:2578–84.
23. Robins HS, Ericson NG, Guenthoer J, O'Briant KC, Tewari M, Drescher CW, et al. Digital genomic quantification of tumor-infiltrating lymphocytes. Sci Transl Med 2013;5:214ra169.
24. Dik WA, Pike-Overzet K, Weerkamp F, de Ridder D, de Haas EF, Baert MR, et al. New insights on human T cell development by quantitative T cell receptor gene rearrangement studies and gene expression profiling. J Exp Med 2005;201:1715–23.
25. Jehs T, Faber C, Juel HB, Bronkhorst IH, Jager MJ, Nissen MH. Inflammation-induced chemokine expression in uveal melanoma cell lines stimulates monocyte chemotaxis. Invest Ophthalmol Visual Sci 2014;55:5169–75.
26. Ayers M, Lunceford J, Nebozhyn M, Murphy E, Loboda A, Kaufman DR, et al. IFN-gamma-related mRNA profile predicts clinical response to PD-1 blockade. J Clin Invest 2017;127:2930–40.
27. Carter SL, Cibulskis K, Helman E, McKenna A, Shen H, Zack T, et al. Absolute quantification of somatic DNA alterations in human cancer. Nat Biotechnol 2012;30:413–21.
28. Bronkhorst IH, Ly LV, Jordanova ES, Vrolijk H, Versluis M, Luyten GP, et al. Detection of M2 macrophages in uveal melanoma and relation with survival. Invest Ophthalmol Vis Sci 2011;52:643–50.
29. Bronkhorst IH, Vu TH, Jordanova ES, Luyten GP, Burg SH, Jager MJ. Different subsets of tumor-infiltrating lymphocytes correlate with macrophage influx and monosomy 3 in uveal melanoma. Invest Ophthalmol Vis Sci 2012;53:5370–8.
30. Medawar PB. Immunity to homologous grafted skin; the fate of skin homografts transplanted to the brain, to subcutaneous tissue, and to the anterior chamber of the eye. Br J Exp Pathol 1948;29:58–69.
31. Campbell M, Humphries P. The blood-retina barrier: tight junctions and barrier modulation. Adv Exp Med Biol 2012;763:70–84.

32. Taylor AW. Ocular immune privilege and transplantation. Front Immunol 2016;7:37.
33. Streilein JW. Ocular immune privilege: therapeutic opportunities from an experiment of nature. Nat Rev Immunol 2003;3:879–89.
34. Triozzi PL, Aldrich W, Singh A. Effects of interleukin-1 receptor antagonist on tumor stroma in experimental uveal melanoma. Invest Ophthal Visual Sci 2011;52:5529–35.
35. Borden EC, Jacobs B, Hollovary E, Rybicki L, Elson P, Olencki T, et al. Gene regulatory and clinical effects of interferon beta in patients with metastatic melanoma: a phase II trial. J Interferon Cytokine Res 2011;31:433–40.
36. Correa D, Somoza RA, Lin P, Schiemann WP, Caplan AI. Mesenchymal stem cells regulate melanoma cancer cells extravasation to bone and liver at their perivascular niche. Int J Cancer 2016;138:417–27.
37. Robledo MM, Bartolomé RA, Longo N, Rodríguez-Frade JM, Mellado M, Longo I, et al. Expression of functional chemokine receptors CXCR3 and CXCR4 on human melanoma cells. J Biol Chem 2001;276:45098–105.
38. Dobner BC, Riechardt AI, Joussen AM, Englert S, Bechrakis NE. Expression of haematogenous and lymphogenous chemokine receptors and their ligands on uveal melanoma in association with liver metastasis. Acta Ophthalmol 2012;90:e638–44.